



Unveiling the adsorption mechanism of organic foulants on anion exchange membrane in reverse electrodialysis using electrochemical methods

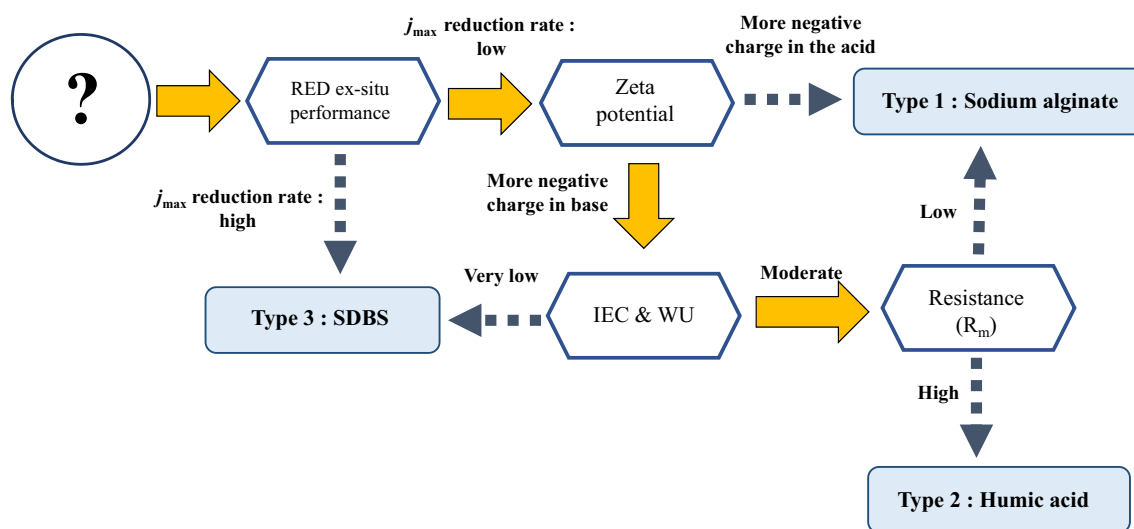
Heajung Song¹ · Insoo Choi^{1,2}

Received: 4 April 2022 / Accepted: 17 November 2022
© The Author(s), under exclusive licence to Springer Nature B.V. 2022

Abstract

This study investigates the fouling of anion exchange membrane by organic foulants in fresh water, which is one of the causes of performance degradation of reverse electrodialysis (RED). Three organic foulants, namely sodium alginate (SA), humic acid (HA), and sodium dodecylbenzene sulfonate (SDBS) are selected and the behavior of adsorption fouling of the selected organic foulants is monitored, analyzed and identified using physicochemical (ion exchange capacity (IEC), water uptake (WU)) and electrochemical (permselectivity, electrochemical impedance spectroscopy (EIS), j - V and j - P plots) methods. Compared to the pristine membrane, the resistance of anion exchange membrane increases and the selective permeability, IEC, and WU decrease after fouling of the membrane, which in turn affects the RED cell performance. SDBS, an aromatic substance, shows a higher adsorption capacity as compared to the other two foulants, and therefore causes severe degradation. Among the two aliphatic substances, namely, HA and SA, HA exhibited higher adsorption capacity than SA because it has fewer carboxylic groups. To summarize, the degradation behavior of the anion exchange membrane was clearly different based on the characteristics of each organic foulant.

Graphical Abstract



Keywords Reverse electrodialysis · Anion exchange membrane · Adsorptive contamination · Organic foulants · Electrochemical property

✉ Insoo Choi
ischoi@kangwon.ac.kr

Extended author information available on the last page of the article

1 Introduction

Since the late 90's renewable energy has attracted strong attention due to energy depletion and climate change. Despite its environmentally benign characteristics, renewable energy suffers from its strong dependence on environmental factors which in turn affects production and utilization [1]. For example, the total power generation and energy conversion efficiency of solar or wind power fluctuate depending on weather conditions. This dependence has supported the emergence of salinity gradient power (SGP) that uses ocean energy due to its relative independence from environmental perturbation. SGP generates electricity using the difference in salt concentration of seawater and fresh water. The theoretical generation of 0.8 kWh from 1 m³ of river water equates to almost 2 TW for the total fresh water flowing from major rivers worldwide [2, 3]. SGP can be divided into pressure retarded osmosis (PRO) and reverse electrodialysis (RED) [4–6].

In a typical RED cell, cation exchange membranes (CEM) and anion exchange membranes (AEM) are alternately stacked, and the spacer between them creates a flow path. When seawater and fresh water are supplied to the compartments divided by the ion exchange membranes (IEMs), the CEM selectively passes the Na⁺ cations and the AEM only transports the Cl⁻ anions, resulting in a voltage due to the difference in the ionic potential. Electrochemical oxidation/reduction reactions of redox species occurring at the electrode generate electricity as electrons move from the anode to the cathode [7, 8]. Increasing the power density of RED requires the reduction of the over-potential applied to the system by developing an efficient electrode or by manufacturing IEM with high co-ion exclusion ability that can reduce the non-ideal permselectivity of the IEM [3, 9].

For technologies using IEMs such as, RED, most research has been focusing on improving the intrinsic properties of the membrane, but mitigating and solving the problem of membrane fouling are also important. Fouling of IEM in RED is mainly caused by chemical and physical interactions of the membrane with foulants present in seawater and fresh water. The fouling increases the membrane resistance and partially degrades the permselectivity, which reduces the RED cell performance [10–12]. Therefore, reducing membrane fouling may improve the stability and durability of RED cell.

Membrane fouling is closely related to the properties of the membrane, i.e., pore structure, surface roughness, and functional group as well as those of the organic foulants, i.e., functional group and surface charge [12–15]. For example, most organic and inorganic foulants have negative and positive surface charge, respectively, which facilitates their attachment to the positively charged AEM and negatively

charged CEM surfaces, respectively. The resulting membrane fouling arising from electrostatic interactions leads to the adsorption of foulants on the membrane surface or entrapment inside the membrane matrix [14, 16, 17]. Vermaas et al. found that fouling caused by natural organic foulants severely affected AEM as compared to CEM, resulting in pressure drop, decrease in open circuit voltage (OCV), and increase in resistance [16]. Another study concluded that natural organic matter (NOM) in rivers decreased the permeability of AEM [18]. Some studies have conducted fouling experiments using fresh water mixed with artificial foulants, rather than natural. Susanto et al. selected bovine serum albumin, sodium alginate (SA) and humic acid (HA) as organic foulants and mixed each one with fresh water [19]. Current density-power (*j*-*P*) curve analysis was applied to evaluate the degradation behavior of CEM and AEM. Fourier transform infrared spectroscopy (FT-IR) and field emission scanning electron microscopy (FE-SEM) confirmed a greater surface adsorption in AEM as compared to CEM. Pintossi et al. compared the ohmic resistance and non-ohmic resistance changes of AEM and CEM before and after membrane fouling by sodium dodecyl benzene sulfonate (SDBS) through electrochemical impedance spectroscopy (EIS) analysis [20].

Previous studies, whether they dealt with NOM or artificial foulants, investigated and compared the performance of RED before and after membrane contamination. Most studies measured the power density and OCV of RED or determined the stack resistance from traditional direct current characterization [16, 18, 19], or AC characterization [20]. Along with performance and resistance-based analyses, a few spectroscopic methods were adopted, such as, UV–visible spectroscopy [18], FT-IR [19], and 2D fluorescence spectroscopy [21]. In addition to study limitations, non-specified NOM or only two contaminants were chosen to induce an adsorptive contamination. Therefore, although these studies concluded with a causal relationship of adsorption fouling by a few contaminants and RED performance in RED systems, they did not investigate the effect of foulant type in their behavioral analysis. Moreover, the characteristics of IEM were not adequately investigated.

RED is a power-generating device which uses ionic transport. Some of the parameters related with ionic transfer in IEM are sensitive to fouling. The adsorption mechanism of organic foulants can be determined by observing changes in the physicochemical and electrochemical parameters of IEM and by deriving the patterns of change. In the present study, we attempted to characterize the IEM-oriented physicochemical (ion exchange capacity (IEC), water uptake (WU), and contact angle) and electrochemical (permselectivity, impedance, and zeta potential) parameters to measure the effect of adsorption contamination on performance as well as to evaluate the correlation between these two

parameters and to unveil the adsorption mechanism. Based on what we envision, it is expected that unknown organic foulants can be revealed by measuring parameters related to membrane properties and by performing inverse inference method, which has not been suggested by any other previous studies. We focused on AEM as it is known to be relatively more susceptible to adsorption than CEM and select three representative organic foulants which can be distinguished by several features. By deriving and categorizing the adsorption behavior of the representative organic foulants, it is expected that effective and unique strategies specific to each categorized foulant will be formulated to reduce or inhibit the fouling of AEM in RED.

2 Materials and methods

2.1 Organic materials and fouling experiment

The three organic foulants were SA ($C_6H_9NaO_7$, JUNSEI chemical), HA ($C_9H_8Na_2O_4$, Sigma-Aldrich), and SDBS ($C_{18}H_{29}NaO_3S$, Sigma-Aldrich). The properties of these organic foulants are summarized in Table 1. SA is extracted from brown algae, and is one of the aliphatic compounds. It represents a group of polysaccharide foulant, which is frequently dealt in the research of membrane contamination. HA is produced from the decomposition of dead plants and is aliphatic compound. It is a representative of humic substance and possesses carboxylic and phenol functional groups, which makes it partially aliphatic and aromatic. HA has fewer carboxylic group than SA, so it is more hydrophobic than SA [22]. SDBS is an aromatic compound with

benzene rings as anionic surfactant. The organic foulants were mixed with 0.5 g L^{-1} NaCl (aq) (Sigma-Aldrich) at a concentration of 1 eq L^{-1} . The zeta potential (ELS-Z, Otsuka Electronics) of the organic foulants was measured to investigate the change of surface charge. By applying a potential to both ends of the cell using a quartz flow cell, the speed of particle movement was measured to obtain a zeta potential value. The pH was adjusted by adding 0.1 M NaOH (Sigma-Aldrich) and 0.1 M HCl (Daejung) to investigate the dependence of zeta potential on pH, and three measurements were averaged.

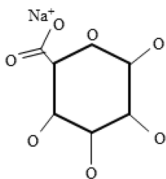
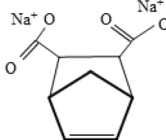
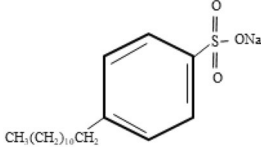
AMV-N (Selemion™, Asahi Glass Co. Ltd., Japan) was used as AEM [23]. In the forced adsorption experiment conducted to observe the degree of fouling, AEM was immersed in a solution containing the organic foulants without stirring to cause intentional fouling. The degradation behavior overtime was investigated at day one, two, and three. The membrane characteristics were measured three times before and after the forced adsorption to obtain reliable results.

2.2 Membrane characterization

Pristine membrane was compared to the fouled membrane with respect to general physicochemical and electrochemical properties. The specific methods were described below.

The IEC measurement of AEM was performed using the Mohr's method [24, 25]. As an indicator, 5 wt% $K_2Cr_2O_7$ (aq) (Sigma-Aldrich) was used according to the following procedure; the AEM was immersed in 1 M NaCl (aq) for 6 h, then taken out and dipped in 100 ml of 2 M NaNO_3 (aq) (Sigma-Aldrich) for 6 h. Then, 50 ml of $NaNO_3$ (aq) in which Cl^- was isolated, was taken out and 0.6 ml of

Table 1 The properties of the three representative organic foulants used in the present study

Organics	Chemical structure	Molecular formula	Molecular weight (g mol^{-1})	Concentration (g L^{-1})
Sodium alginate		$C_6H_9NaO_7$	216.12	1
Humic acid		$C_9H_8Na_2O_4$	226.14	1
SDBS		$C_{18}H_{29}NaO_3S$	348.48	0.76

$K_2Cr_2O_7$ was added to the solution. If a titration solution, 0.1 M $AgNO_3$ (aq) (Sigma-Aldrich) was added to the mixture solution, a white precipitate was formed. The volume of $AgNO_3$ was measured when the color of mixture solution turned from yellow to reddish brown. IEC was calculated using Eq. (1).

$$IEC \left(\frac{\text{meq}}{\text{g}} \right) = \frac{2 \times N_{AgNO_3} \times V_{AgNO_3}}{W_{\text{dry}}} \quad (1)$$

N_{AgNO_3} is the normality, V_{AgNO_3} is the volume of $AgNO_3$ solution, and W_{dry} is the weight of the dry membrane which has been dried at 50 °C for 6 h in a vacuum oven. The factor of 2 is applied because the solution in which the AEM was immersed is 100 mL and then is changed to 50 mL when titrated.

WU is commonly referred to as the swelling degree (SD) or water content [26]. WU is an important indicator for membrane dimensional stability and ionic transport properties, and has a positive effect on the membrane conductivity [2, 27]. The WU of AEM was measured as follows; after dipping the AEM in deionized water, the water was quickly wiped off with tissue paper and the AEM was weighed (W_{wet}). The AEM was dried in a vacuum oven at 50 °C for at least 6 h and then weighed (W_{dry}). WU of the AEM was calculated according to the following equation [28].

$$WU = \frac{W_{\text{wet}} - W_{\text{dry}}}{W_{\text{dry}}} \times 100 \quad (2)$$

The permselectivity of the membrane is generally determined by the potential difference of the membrane in the concentration polarization of the solution [2]. To measure

the permselectivity, as shown in Fig. 1a, the two compartments were divided by a membrane to form a two-electrode system. A solution of 30 g L^{-1} NaCl and 0.5 g L^{-1} NaCl was added to each compartment. The membrane potential was measured by reading the open circuit potential (OCP) between the saturated calomel electrode (SCE) which was used as the reference electrode in the two compartments with a potentiostat (PGSTAT302N, Autolab). The membrane area was 2 cm^2 and the OCP was measured when the membrane potential reached equilibrium. The permselectivity of the membrane was calculated according to the following equation.

$$\text{Permselectivity} = \frac{E_{\text{meas}}}{E_{\text{theo}}} \times 100\% \quad (3)$$

E_{meas} is the potential difference measured by experiments and E_{theo} is the theoretically calculated potential difference. The E_{theo} was calculated according to the following equation.

$$E_{\text{theo}} = \alpha_{\text{AEM}} \frac{RT}{zF} \ln \frac{r_H C_H}{r_L C_L} \quad (4)$$

where α_{AEM} is the apparent membrane permselectivity, R is the gas constant ($J \text{ mol}^{-1} \text{ K}^{-1}$), T is the absolute temperature (K), z is electrochemical valence, F is the Faraday constant ($C \text{ mol}^{-1}$), r_H and r_L mean activity coefficient of sodium and chloride ion in high-salinity and low-salinity water, C_H and C_L are concentration of high-salinity and low-salinity water (mol L^{-1}) [29].

Membrane resistance is an important parameter determining energy-generating performance in RED cells [9]. As shown in Fig. 1b, the membrane resistance was determined

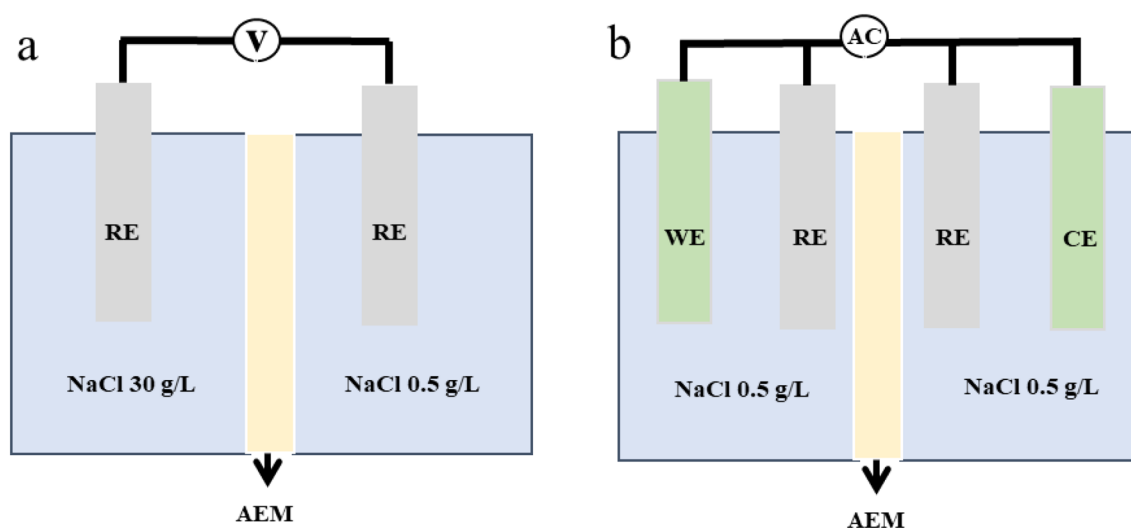


Fig. 1 Apparatus for measuring electrochemical properties of membrane: **a** two-electrode system for permselectivity, **b** four-electrode system for impedance, where RE, CE, and WE refer to the reference electrode, counter electrode, and working electrode, respectively

by EIS analysis in a four-electrode system. The membrane area was 2 cm². Ti foil was used as the working electrode (WE) and the counter electrode (CE), and a saturated calomel electrode (in 3 M KCl) in a Luggin-Haber capillary was used as the reference electrode (RE). Before the resistance measurement, the membrane was equilibrated by soaking it in fresh water 0.5 g L⁻¹ NaCl solution for at least 24 h. The EIS measurement was performed in the frequency range of 10⁻¹–10⁶ kHz, and the amplitude was set a 1 mV. The membrane resistance (R_m) was derived by subtracting the measured resistance (R_s) when there was only a solution without a membrane, from the measured resistance (R_{s+m}), when the membrane and the solution were in contact. This can be expressed in the following equation:

$$R_m (\Omega \text{ cm}^2) = R_{s+m} - R_s (\Omega) \times A (\text{cm}^2) \quad (5)$$

The membrane surface was analyzed by FE-SEM (JSM-6701F, X-Max) to determine whether and how much organic foulants were adsorbed. An energy dispersive X-ray spectroscopy (EDS) elemental mapping image was obtained by analyzing the membrane sample dried at 50 °C for more than 6 h in a vacuum oven using FE-SEM. The degree of hydrophobicity of the membrane surface was measured using the sessile drop technique (D04010 Easy drop, KRUSS). Finally, atomic force microscope (AFM, XE-150, Park systems) was conducted in the non-contact mode to determine the root mean square (RMS) roughness of the membrane surface before and after membrane fouling from the 1 μm² membrane area.

2.3 RED performance measurement

A RED single cell (7 × 7 cm²) with an electrode area of 9 cm² was constructed using CMV-N (SelemionTM, Asahi Glass Co. Ltd., Japan) as a CEM and AMV-N as an AEM (active area = 11.25 cm²). Ti woven spacer (The Nilaco corporation, thickness = 200 μm) was inserted to form a flow channel between the membranes, and the spacer was surrounded by a Teflon gasket (thickness = 280 μm). Pt-deposited Ti mesh was employed as electrode and placed at the end of cell. The full schematic of RED single cell is provided in Figure S1. The feed water solutions were prepared by dissolving NaCl in deionized water. The concentration of low-salinity water (C_L) and high-salinity water (C_H) was fixed at 0.5 g L⁻¹ NaCl and 30 g L⁻¹ NaCl, respectively. Both high- and low-salinity water were supplied to the RED cell at 5 mL min⁻¹ by peristaltic pump (Masterflex®, Cole-Parmer). The specific materials and cell structure were described in previous studies [30, 31]. When examining the fouling performance in the presence of organic foulants, the C_H was kept constant, and 1 eq L⁻¹ of organic foulants was added to low-salinity water. The performance of the RED

single cell was measured using potentiostat. The j - V and j - P curves were obtained from galvanodynamic operation until the voltage decreased to zero at a current rate of 0.1 mA s⁻¹ to compare the performance of RED cells before and after membrane fouling.

3 Results and discussion

3.1 *Ex situ* performance of RED with foulants

Prior to investigating the effects of foulants on the properties of AEM, the degradation behavior of RED single cell as a function of fouling time was examined and compared. *Ex situ* method was applied to RED cell using the three organic foulants. The *ex situ* method refers to an experiment in which AEM was pre-adsorbed by foulants and was embedded to RED cell to evaluate its performance. Organic foulants (1 eq L⁻¹) was added to low-salinity water. The organic-mixed solution was used because the flow of fresh water could wash the fouled AEM and so the organic-mixed solution was added as a flow during the measurement time (10 min), as well as the activation time. The *ex situ* performance of RED with different foulants with a j - V curve is shown in Fig. 2. OCV and j_{max} (maximum current density generated by RED cell) are summarized in Table S1. The performance of RED cell decreased with fouling time in the presence of all organic foulants, implying that the foulants induced adsorptive contamination of AEM and degraded the performance of RED. However, the degree of degradation was different for each foulant. After 3 days, OCV and j_{max} decreased by 5% and 25%, respectively, for SA and by 6% and 31%, respectively, for HA. SDBS, an aromatic compound, exhibited the largest performance reduction with 91% for OCV and 99% for j_{max} . On the other hand, HA and SA, which are aliphatic hydrocarbon compounds, exhibited lower performance reduction. It is noteworthy highlighting that HA, with fewer carboxylic groups, showed slightly greater performance reduction than SA. To summarize, the degree of degradation decreased in the following order: SDBS > HA > SA.

SEM-EDS elemental mapping analysis of AEM pre-adsorbed by organic foulants was conducted to observe the tendency and extent of adsorptive fouling of the membrane (Figure S2–S4). It was evident that the organic foulant adsorption on the AEM surface was positively correlated with fouling time. For SA and HA, C and O were chosen as indicative atoms for comparison, while S and O were selected for SDBS. AEM fouling was pronounced with longer fouling time, but each organic foulant exhibited a different degradation behavior. There was no significant difference in the SEM-EDS mapping analysis, but the *ex situ* RED performance differed significantly, which confirmed

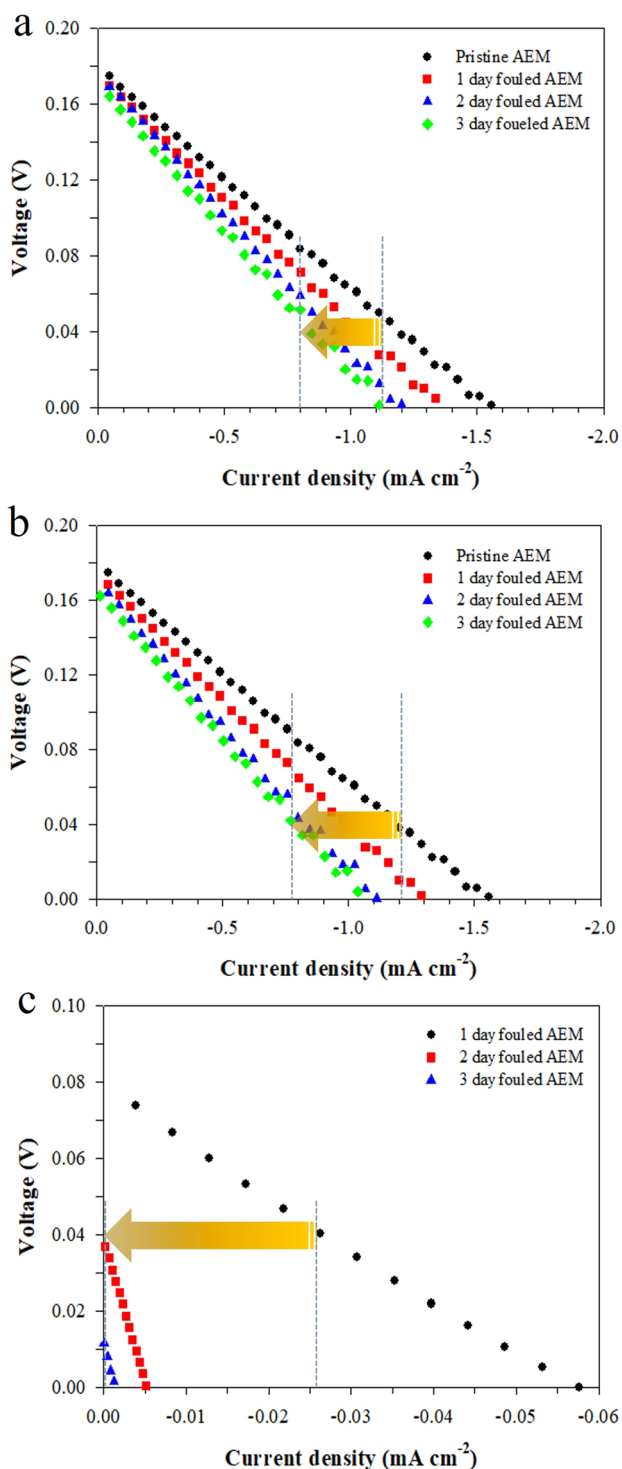


Fig. 2 *Ex situ* performance of RED single cell embedded with a fouled AEM using **a** SA, **b** HA, and **c** SDBS

the limitation in using physicochemical methods to determine the degradation behavior of each organic foulant. In order to more precisely determine the degradation behavior of each organic foulant, the mechanisms and characteristics

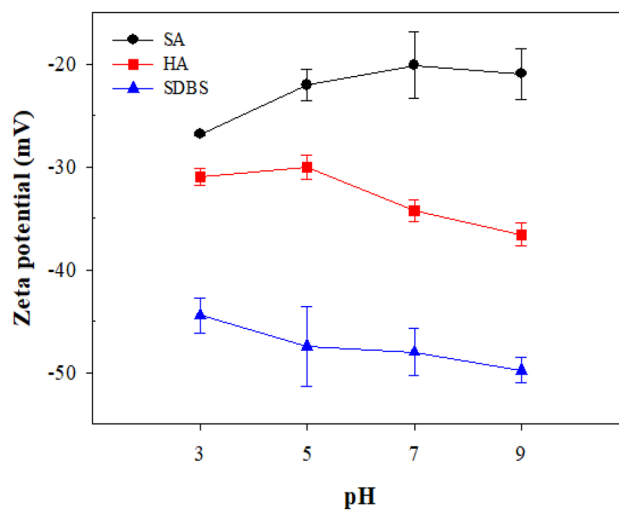


Fig. 3 Zeta potential of the three organic foulants dissolved solution with various pH

by which the organic foulants affected the AEM degradation were examined using electrochemical methods.

3.2 Zeta potential of organic foulants

Zeta potential is an interfacial electrochemical parameter that governs the electrostatic interaction between organic foulants and IEM [32]. The electrostatic force of organic foulants and membrane can cause membrane fouling. Since the cationic functional group is fixed on the surface of the AEM, the zeta potential of the AEM is 6.4 mV [33]. The higher the negative charge of the organic foulants, the stronger the interaction between the AEM and the organic foulants, which increases the adsorption contamination. Therefore, varying zeta potential of organic foulants will affect the degradation behavior because the degree of electrostatic attraction between the organic foulants and AEM is different and the degree of fouling can be predicted in advance. Figure 3 shows the zeta potential of organic foulants according to the pH of the solution. As can be seen, all foulants had high negative charges and would be easily adsorbed onto the positively charged AEM surface, causing membrane fouling. It was noted that for HA and SDBS zeta potential decreased with increasing pH, while it increased with increasing pH for SA. At all pH levels, the zeta potential increased in the following order SDBS > HA > SA. The *ex situ* performance of RED was conducted at pH 7, where the zeta potential of the foulant was -20 mV, -36 mV, and -48 mV for SA, HA, and SDBS, respectively. Therefore, the magnitude of electrostatic interaction and the degree of surface adsorption were positively correlated. SDBS had the highest negative surface charge, so it can be inferred that the adsorption behavior of SDBS was largely due to electrostatic

interaction. In addition, the SDBS aromatic matrix assumes the participation of this foulant not only in electrostatic, but also in stacking interaction. It is π - π stacking interaction that can cause the maximum growth of negative zeta potential values in the case of SDBS compared to other foulants. The zeta potential analysis suggested that electrostatic interaction was the primary reason for adsorption of IEM by organic species.

3.3 Ion exchange capacity (IEC) and water uptake (WU)

IEC is a parameter indicating the number of cationic functional groups fixed on the IEM surface and is used as a factor to evaluate the ion exchange capacity of the IEM. IEC largely determines the transport characteristics of IEM (electrical conductivity, permeability, permselectivity) [5]. This is why the magnitude of the IEC changes is used to predict the behavior of the AEM after fouling. The IEC values before and after membrane fouling are shown in Fig. 4a using Eq. (1). Fouled AEM from the forced adsorption

fouling experiment showed decreased IEC compared to pristine AEM according to the fouling time in all organic matter. Furthermore, the IEC decrement increased for longer fouling duration, which suggested an accelerated adsorptive contamination. After 3 days, IEC decreased by 30%, 35%, and 50% for SA, HA, and SDBS, respectively, compared to pristine AEM. This means that the $-NR_3^+$ cation functional group fixed on the AMV-N surface was reduced due to adsorptive contamination of organic foulants, and the membrane lost its ion exchange capacity. The degree of decrement in IEC was the greatest for SDBS, highlighting largest electrostatic interaction with AEM.

Considering that water content affects ion transport, such as, diffusion and migration, WU is an important factor for analyzing IEM performance [5]. The IEM should be sufficiently hydrated for effective ion transfer. The change of WU before and after membrane fouling is shown in Fig. 4b using Eq. (2). Like IEC, WU also decreased after membrane fouling. The decreasing trend of WU was attributed to the degree of fouling, which could be explained by changes in structural and surface properties of IEM caused by adsorptive contamination. The adsorption of foulants on the pore walls of the membrane, driven by the aforementioned electrostatic interaction, leads to screening of hydrated fixed groups. In addition, the formation of colloidal particles of foulants inside the pores can reduce the free volume of the membrane. The structural change is notable when SDBS is involved, because there occurs stacking interaction as well as electrostatic interaction and the critical micelle concentration of SDBS ($0.612 \mu\text{M}$) is much lower than that of HA and SA ($4.5 \sim 5 \text{ mM}$). Besides, the change in surface property also affected the trend in WU. When hydrophobic organic matter was adsorbed on substrate, the substrate surface changed to hydrophobic. The contact angle measurement results in Table S2 and Figure S5 reflected the hydrophobic characteristic of IEM. After 3 days, the contact angle of organic-adsorbed IEM surface increased in the following order SDBS > HA > SA. WU decreased as the surface hydrophobicity of fouled AEM increased. This increasing hydrophobicity of the AEM surface prevented the membrane from absorbing water, and this ultimately reduced the water content thereby decreasing the ionic conductivity. The reduction in IEC and WU increased in the following order of SDBS > HA > SA. This is because SDBS, which has the greatest negative zeta potential, showed a strong adsorption tendency, followed by fouling tendency. In conclusion, different degradation behaviors in the *ex situ* RED were related to the zeta potential of organic foulants with different negative charge values, which was supported by the corresponding reduction tendency of IEC and WU.

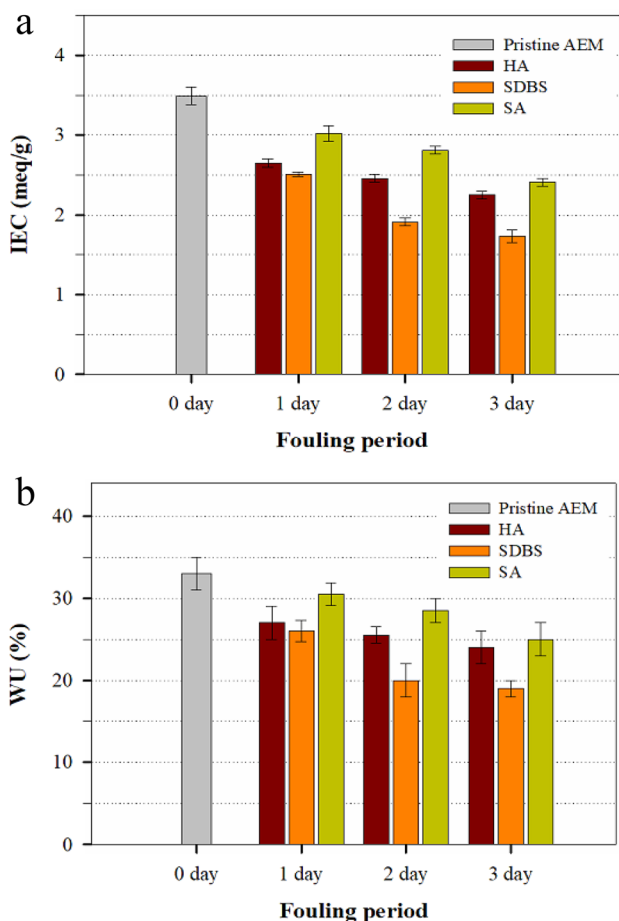


Fig. 4 **a** Ion exchange capacity and **b** water uptake of a fouled AEM by the three organic foulants according to fouling time

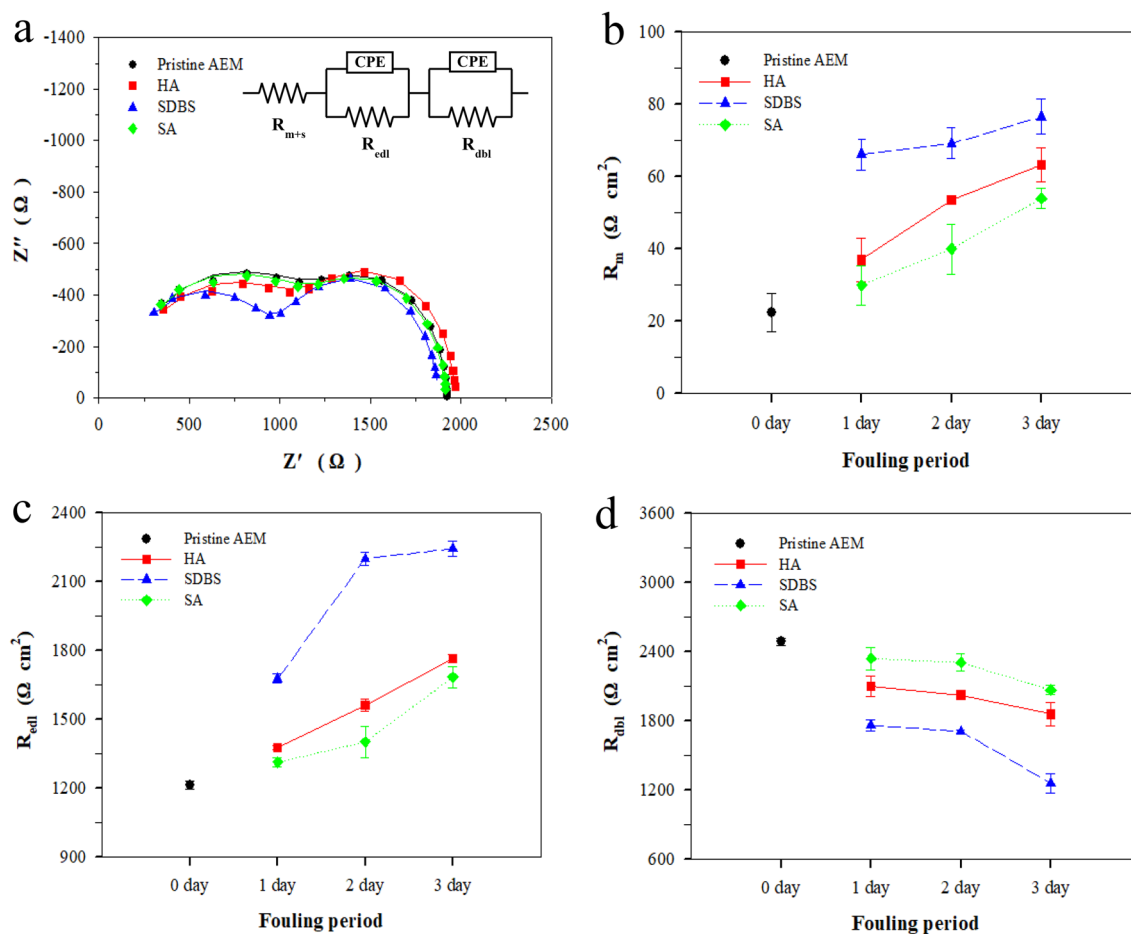


Fig. 6 The results of electrochemical impedance spectroscopy analysis: **a** Nyquist plots of 1 day-fouled and pristine AEM (inset: equivalent circuit) **(b)** membrane resistance **(c)** electric double layer

resistance, and **d** diffusion boundary layer resistance of a fouled and pristine AEM according to fouling time

3.4 Permselectivity

Permselectivity is used to measure the ability of the membrane to selectively transport counter-ion and exclude co-ion.

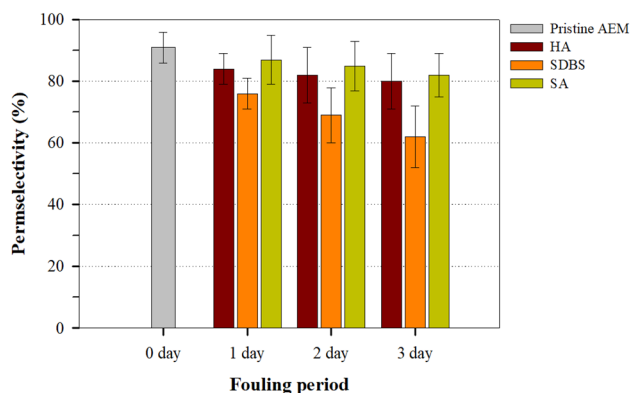


Fig. 5 Permselectivity of a fouled AEM by the three organic foulants according to fouling time

In general, a perfect IEM can have a permselectivity of 100% when the co-ion is completely excluded from the membrane, but according to Donnan's theory, some co-ions contribute to the transport current [34]. Therefore, the permselectivity will decrease below the ideal value of 1 [26]. Figure 5 shows the results obtained using a two-electrode system which is shown in Fig. 1a, for the permselectivity before and after membrane fouling. Firstly, the permselectivity of pristine AEM was found to be 91%. After 3 days of fouling, the value decreased by 9%, 12%, and 31% for SA, HA, and SDBS, respectively. As expected, this decline trend was similar to that of IEC and WU. In general, the co-ion exclusion decreased when the IEC was low and the expansion of the membrane was larger, resulting in a lower permselectivity [35]. Therefore, since the flow of counter-ion through the membrane was determined by the fixed charge density of the membrane, it was consistent with previous study results which suggested that a small IEC value reduced the permselectivity [9, 35, 36]. In addition, permselectivity is important

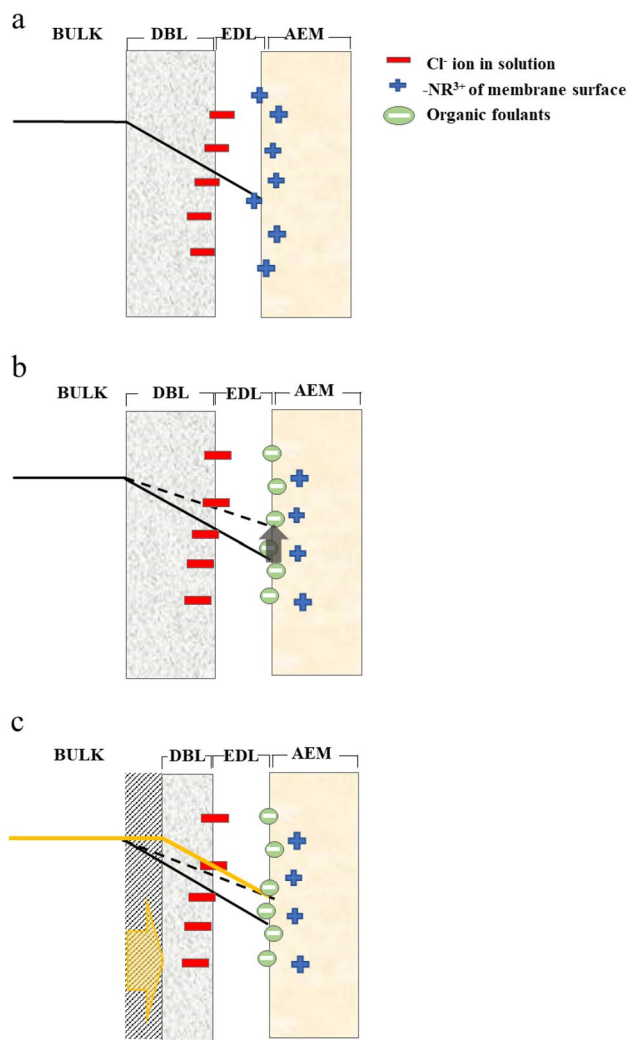


Fig. 7 A schematic of concentration polarization of anion near the interface between AEM and solution: **a** before fouling, **b** after fouling, and **c** change in diffusion boundary layer upon fouling. The solid and dash lines refer to the anion concentration before and after contamination, respectively

in the RED system because the OCV of the RED cell was determined according to the following Nernst equation [30].

$$E_{\text{OCV}} = \alpha_{\text{CEM}} \frac{RT}{F} \ln \frac{\gamma_{\text{H}}^{\text{Na}^+} C_{\text{H}}}{\gamma_{\text{L}}^{\text{Na}^+} C_{\text{L}}} + \alpha_{\text{AEM}} \frac{RT}{F} \ln \frac{\gamma_{\text{H}}^{\text{Cl}^-} C_{\text{H}}}{\gamma_{\text{L}}^{\text{Cl}^-} C_{\text{L}}} \quad (6)$$

According to the above equation, the permselectivity of the IEM (α_{CEM} , α_{AEM}) is one of the variables that determine the OCV of a cell. Thus, the reduction and the reduction tendency of OCV after fouling in the *ex situ* RED performance reported in Table S2 were due to a change in permselectivity by different organic foulants.

3.5 Impedance analysis

The EIS was conducted to further investigate changes in properties of IEM due to adsorptive contamination and to unveil why and how adsorption occurred depending on the type of organic foulants. EIS provides information on the area resistance of IEM. Unlike the direct current (DC) method, EIS is widely used to investigate the electrochemical properties of IEM because it can quantify individual values of resistance [37]. As shown in Fig. 1b, a four-electrode system was used to measure the resistance of the AEM before and after membrane fouling. The quantitative value of each resistance element was found by fitting the equivalent circuit of Fig. 6a and the results are summarized in Fig. 6b–d (R_{m} , R_{edl} , R_{dbl}). R_{m} is the resistance of the IEM and R_{edl} is the resistance of the electrical double layer (EDL) in which ions are bound to IEM by electrostatic interaction. The EDL is composed of two layers namely, an inner layer, called Stern layer (SL) which is formed by ions strongly bound by electrostatic interactions with the membrane surface, and an outer layer, called diffuse layer (DL) which is constituted of loosely bonded ions. R_{dbl} refers to the resistance of the diffusion boundary layer (DBL) which is created by the difference in the number of ions transported between the solution and the IEM [38]. The R_{m} of fouled AEM increased compared to that of pristine AEM and this was attributed to the formation of adsorption layer on the IEM surface or to pores blocked by organic foulants [13, 14]. Previous studies have reported that SA and HA could possibly block the pores of the membrane during membrane filtration for water purification [39]. This suggests that the aliphatic compounds HA and SA were adsorbed on the membrane surface and blocked the pores of the membrane during reverse electro dialysis, thereby increasing R_{m} . The resistance of SDBS, an aromatic compound, was much higher than that of the other two organic foulants because it formed a micelle with surfactants, which increased the fouling severity [40]. Therefore, the R_{m} increased in the following order SDBS > HA > SA.

R_{edl} exhibited a similar tendency to that of R_{m} . As organic foulants are electronegative, foulants are adsorbed on the IEM surface, and salt ions and organic foulants competed in the double layer of the AEM, thus decreasing the process performance [41]. Eventually, as the membrane fouling increased, the concentration of counter-ion in the EDL of the IEM increased compared to the pristine AEM, thus the R_{edl} increased as the range of the EDL region increased. In addition, it is possible that the thickness of the EDL increased due to the interfacial contact between the electrolyte and the AEM, as organic foulants were adsorbed onto the AEM surface which became hydrophobic. This might also be due to obstruction of the AEM pores by organic foulants which

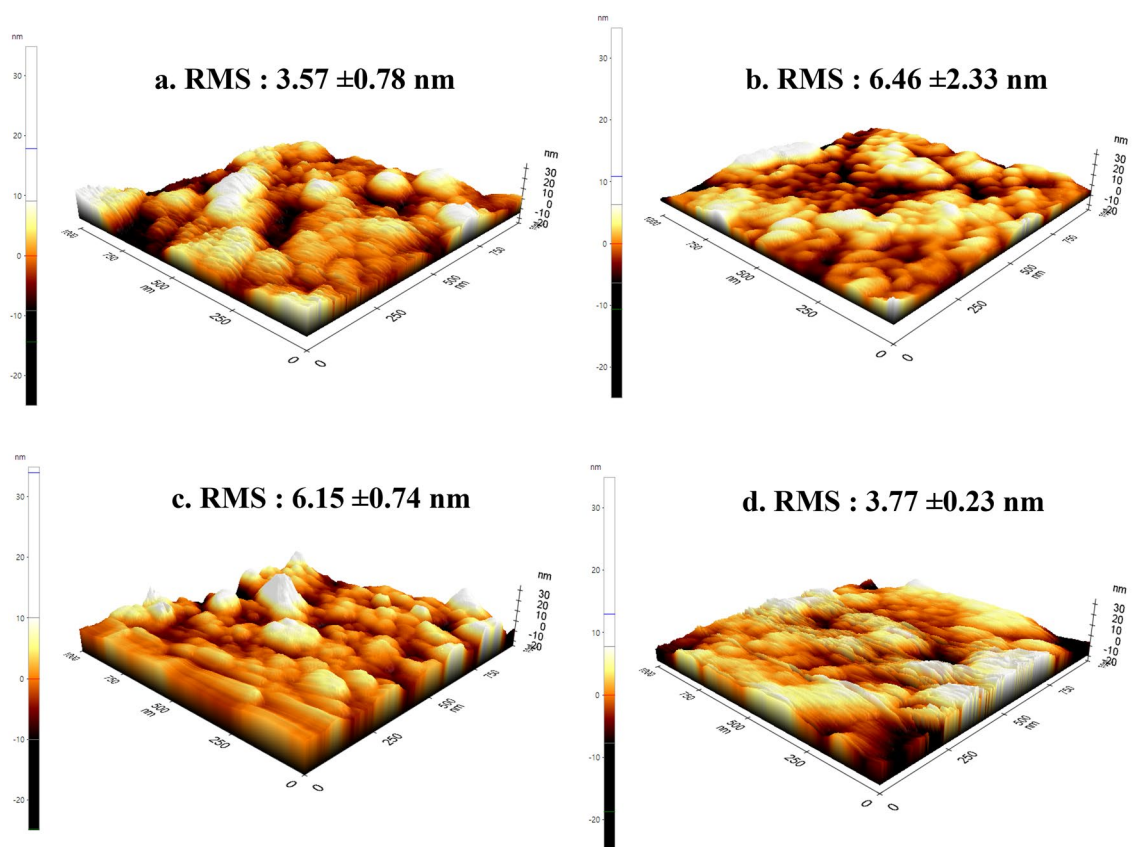


Fig. 8 AFM 3D images of **a** pristine, **b** SA-fouled, **c** HA-fouled, and **d** SDBS-fouled AEM

impeded the flow of smooth ions through the pores, thereby increasing the R_{edl} .

In the case of R_{dbl} , unlike the previous resistances, the resistance after membrane fouling decreased as compared to that of pristine AEM. A previous study reported a similar result due to negatively charged organic foulants that weakened the concentration polarization at the interface between the membrane and the solution, as shown in Fig. 7a–c [41]. Before fouling, a concentration polarization was formed by the positive charge fixed on the AEM surface and the Cl^- ion contained in the solution (Fig. 7a). Then, AEM fouling decreased the amount of positive charge, and the concentration polarization weakened as organic foulants with negative charges were adsorbed on the surface (Fig. 7b). During measurement, the same electric load was applied and therefore the concentration polarization was recovered, restoring the concentration gradient. Since the bulk concentration did not change, the thickness of DBL should have decreased, ultimately reducing R_{dbl} (Fig. 7c). Figure 8 is an AFM measurement image of a membrane in which AEM was immersed in organic foulants for one day. The surface roughness of the membrane was determined from the AFM measurement to indicate the degree of cleanliness of the film surface, as the surface roughness value was negatively correlated with

the degree of foulants accumulation on the AEM surface [42]. The surface roughness increased in the following order $\text{SA} > \text{HA} > \text{SDBS}$, indicating that SDBS covered the AEM surface thickest, followed by HA and SA. Therefore, R_{dbl} increased in the following order $\text{SA} > \text{HA} > \text{SDBS}$. Although some previous studies have drawn similar conclusions, non-ohmic resistance has not been specified [20], or it has been summarized simply by the influence of hydrodynamic [19]. However, in this study, the detail description of fouling by various foulant was possible by deriving the resistance component of non-ohmic resistance, R_{EDL} and R_{DBL} .

3.6 RED single cell *in situ* performance

Following the aforementioned investigation into the characteristics of AEM before and after fouling with organic foulants, in this section the performance of the RED cell under real operating conditions was investigated using a pristine AEM by adding a flow of feed solution containing organic foulants. The C_{H} was fixed and a mixture of $C_{\text{L}} + 1 \text{ eq L}^{-1}$ SA, HA, and SDBS was supplied. The performance was measured as the fouling progressed. Figure 9 shows the results of the j - P curve measured for 24 h *in situ*. The performance decrement for SDBS was too significant

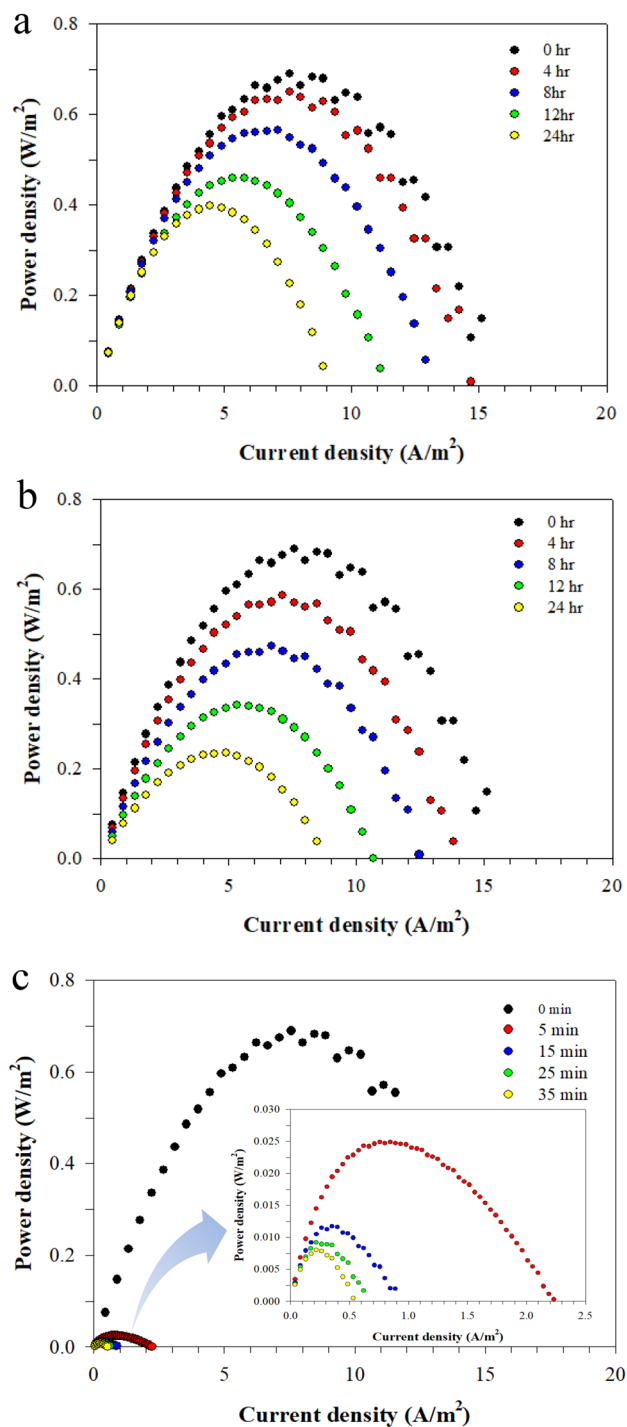


Fig. 9 *In situ* performance of RED single cell embedded with a fouled AEM by (a) SA, (b) HA, and (c) SDBS

and fast to be measured for 24 h. When organic mixture was used for 24 h, P_{\max} (the maximum power density that can be generated in RED cell) decreased by 41% for SA, 65% for HA, and 98% for SDBS in 35 min, as compared to AEM. Even under real operating conditions, the degradation behavior of the organic foulants showed similar results to the

ex situ experiment following this order SDBS > HA > SA. However, the *in situ* method showed a greater performance decrement than the *ex situ* method in a short period of time because of the pumped flow of organic foulants. Whereas in the *ex situ* method, the AEM was immersed in static organic foulants without stirring. Additionally, as shown in Figure S6, HA was trapped in the pores of the spacer and membrane after the *in situ* experiment but not in the *ex situ* condition. Because the pore filling of the spacer by organic foulants was accelerated in the *in situ* mode, the *in situ* RED performance was lower than the *ex situ* performance. In addition, the continuous flow of organic foulants extended the contact time between the cell components and the organic foulants, which raised the likelihood that the AEM and other components became contaminated.

3.7 Categorizing adsorptive contamination

HA, which has fewer carboxylic functional groups, is a representative hydrophobic organic material and is more susceptible to fouling of the membrane than SA. HA attaches to the AEM surface by electrostatic attraction, making the AEM surface hydrophobic, thus leading to membrane fouling as a result of hydrophobic interaction between the membrane and organic matter. Therefore, the greater hydrophobicity of the AEM surface hindered the penetration of the ions of the feed solution into the membrane, which increased resistance and reduced performance.

SA with more carboxylic functional groups is more hydrophilic than HA and has a lower molecular weight. It can be more easily trapped inside the membrane matrix based on geometric interaction and can be adsorbed into the interior or onto the membrane surface by electrostatic interaction [43, 44]. In addition, compared to HA, SA weakly attaches to the membrane surface due to the repulsive force between the slightly hydrophilic organic foulants and the hydrophobic membrane.

SDBS, an aromatic compound with a benzene ring, was associated to the most fouled and most severely degraded RED performance. According to Tanaka et al. the fouling of aromatic foulants and aromatic membrane was the more severe than other cases based on the following order; aromatic foulants-aromatic AEM > aliphatic foulants-aromatic AEM > aliphatic foulants-aliphatic AEM [11, 14]. The AEM used in this experiment was an aromatic membrane and was related to severe membrane contamination due to greatest aromatic SDBS affinity interaction (π - π stacking).

4 Conclusion

Three organic foulants, namely, SA, HA, and SDBS were mixed with fresh water to analyze the resulting AEM fouling. The fouling behavior was investigated by physicochemical and electrochemical properties. The zeta potential measurement revealed negative charges on the three organic foulants and hence their potential to foul the AEM. The magnitude of the negative charges decreased in the following order SDBS > HA > SA. SDBS, an aromatic material, had the strongest electrostatic attraction with the membrane, and showed higher adsorption capacity on the AEM surface as compared to the other two foulants, due to affinity interaction with the aromatic membrane. The AFM analysis revealed that SDBS formed a dense and more extensive fouling layer, which more strongly degraded the RED single cell performance. According to the AFM results, aliphatic substances HA and SA were more densely attached to the surface than SDBS. In addition, HA showed a higher adsorption capacity than SA, because HA which possessed fewer carboxylic groups was fouled by hydrophobic interaction with AEM. In the *in situ* method, HA caused fouling of both the membrane and the spacer which affected the performance reduction of the RED cell. SA with more carboxylic functional groups was relatively reversible to contamination due to the repulsive force between the slightly hydrophilic organic and the hydrophobic membrane. To summarize the study findings, the degradation behavior of AEM following membrane fouling varied according to the different characteristics of the three organic foulants. Therefore, different cleaning or anti-contamination strategies could be formulated and used for each type of organic foulant. This study is meaningful compared to the previous ones in that (1) the organic foulants are categorized based on their chemical structure and property; (2) the electrochemical analysis are thoroughly conducted to supplement the physicochemical analysis; (3) the hydrodynamic upon fouling are described and it is used to differentiate the fouling behavior with respect to the class of foulant; (4) a correlation between membrane parameters and foulant property is made so that unknown organic foulants can be revealed by measuring parameters related to membrane properties and by performing inverse inference method.

Supplementary Information The online version contains supplementary material available at <https://doi.org/10.1007/s10800-022-01816-5>.

Acknowledgements The research was supported by the Ministry of Science and ICT through the National Research Foundation of Korea (NRF-2022R1C1C1013043) and was also funded by the Korea Electric Power Corporation (Grant number: R19X001-02).

References


1. Connolly D, Lund H, Mathisen BV, Pican E, Leahy M (2012) The technical and economic implications of integrating fluctuating renewable energy using energy storage. *Renew Energy* 43:47–60. <https://doi.org/10.1016/j.renene.2011.11.003>
2. Mei Y, Tang CY (2017) Recent developments and future perspectives of reverse electrodialysis technology: a review. *Desalination* 425:156–174. <https://doi.org/10.1016/j.desal.2017.10.021>
3. Logan BE, Elimelech M (2012) Membrane-based processes for sustainable power generation using water. *Nature* 488:313–319. <https://doi.org/10.1038/nature11477>
4. Kwak SH, Kwon SR, Beak S, Lim SM, Joo YC, Chung TD (2016) Densely charged polyelectrolyte-stuffed nanochannel arrays for power generation from salinity gradient. *Sci Rep* 6:26416. <https://doi.org/10.1038/srep26416>
5. Veerman J, Saakes M, Metz SJ, G.J. (2009) Harmsen. Reverse electrodialysis: performance of a stack with 50 cells on the mixing of sea and rive water. *J Membr Sci* 327:136–144. <https://doi.org/10.1016/j.memsci.2008.11.015>
6. Post JW, Veerman J, Hamelers HVM, Euverink GJW, Metz SJ, Nymeijer K, Buisman CJN (2007) Salinity-gradient power: evaluation of pressure-retarded osmosis and reverse electrodialysis. *J Membr Sci* 288:218–230. <https://doi.org/10.1016/j.memsci.2006.11.018>
7. Dlugolecki P, Nymeijer K, Metz S, Wessling M (2008) Current status of ion exchange membranes for power generation from salinity gradients. *J Membr Sci* 319:214–222. <https://doi.org/10.1016/j.memsci.2008.03.037>
8. Post JW, Hamelers H, Buisman CJN (2008) Energy recovery from controlled mixing salt and fresh water with a reverse electrodialysis system. *Environ Sci Technol* 42:5785–5790. <https://doi.org/10.1021/es8004317>
9. Guler E, Elizen R, Vermaas D, Saakes M, Nijmeijer K (2013) Performance-determining membrane properties in reverse electrodialysis. *J Membr Sci* 446:266–276. <https://doi.org/10.1016/j.memsci.2013.06.045>
10. Chang DI, Choo KH, Jung JH, Jiang L, Ahn JH, Nam MY, Kim ES, Jeong SH (2009) Foulant identification and fouling control with iron oxide adsorption in electrodialysis for the desalination of secondary effluent. *Desalination* 236:152–159. <https://doi.org/10.1016/j.desal.2007.10.062>
11. Tanaka N, Nagase M, Higa M (2011) Preparation of aliphatic-hydrocarbon-based anion exchange membranes and their anti-organic-fouling properties. *J Membr Sci* 384:27–36. <https://doi.org/10.1016/j.memsci.2011.08.064>
12. Li Q, Song J, Yu H, Li ZK, Pan XH, Yang B (2014) Investigating the microstructures and surface features of seawater RO membranes and the dependencies of fouling resistance performances. *Desalination* 352:109–117. <https://doi.org/10.1016/j.desal.2014.08.015>
13. Xu H, Xiao K, Wang X, Liang S, Wei C, Wen X, Huang X (2020) Outlining the roles of membrane-foulant and foulant-foulant interactions in organic fouling during microfiltration and ultrafiltration—a mini-review. *Front Chem*. <https://doi.org/10.3389/fchem.2020.00417>
14. Tanaka N, Nagase M, Higa M (2012) Organic fouling behavior of commercially available hydrocarbon-based anion-exchange membranes by various organic-fouling substances. *Desalination* 296:81–86. <https://doi.org/10.1016/j.desal.2012.04.010>
15. Park JS, Lee HJ, Moon SH (2003) Determination of an optimum frequency of square wave power for fouling mitigation in desalting electrodialysis in the presence of humate. *Sep Purif Technol* 30:101–112. [https://doi.org/10.1016/S1383-5866\(02\)00138-7](https://doi.org/10.1016/S1383-5866(02)00138-7)

16. Vermaas DA, Kunteng D, Saakes M, Nijmeijer K (2013) Fouling in reverse electrodialysis under natural conditions. *Water Res* 47:1289–1298. <https://doi.org/10.1016/j.watres.2012.11.053>
17. Li HG, Xia HJ, Mei YX (2016) Modeling organic fouling of reverse osmosis membrane: from adsorption to fouling layer formation. *Desalination* 386:25–31. <https://doi.org/10.1016/j.desal.2016.02.037>
18. Kingsbury RS, Liu F, Zhu S, Boggs C, Armstrong MD, Call DF, Coronell O (2017) Impact of natural organic matter and inorganic solutes on energy recovery from five real salinity gradients using reverse electrodialysis. *J Membr Sci* 541:621–632. <https://doi.org/10.1016/j.memsci.2017.07038>
19. Susanto H, Fitrianingtyas M, Samsudin AM, Syakur A (2017) Experimental study of the natural organic matters effect on the power generation of reverse electrodialysis. *Int J Energy Res* 41:1474–1486. <https://doi.org/10.1002/er.3728>
20. Pintossi D, Saakes M, Borenman Z, Nijmeijer K (2019) Electrochemical impedance spectroscopy of a reverse electrodialysis stack: a new approach to monitoring fouling and cleaning. *J Power Sources* 444:227302. <https://doi.org/10.1016/j.jpowsour.2019.227302>
21. Pawlowski S, Galinha CF, Crespo JG, Velizarov S (2016) 2D fluorescence spectroscopy for monitoring ion-exchange membrane based technologies – Reverse electrodialysis (RED). *Water Res* 88:184–198. <https://doi.org/10.1016/j.watres.2015.10.010>
22. Zhao F, Xu K, Ren H, Ding L, Geng J, Zhang Y (2015) Combined effects of organic matter and calcium on biofouling of nanofiltration membrane. *J Membr Sci* 486:177–188. <https://doi.org/10.1016/j.memsci.2015.03.032>
23. Le XT, Bui TH, Viel P, Berthelot T, Palacin S (2009) On the structure-properties relationship of the AMV anion exchange membrane. *J Membr Sci* 340:133–140. <https://doi.org/10.1016/j.memsci.2009.05.025>
24. Lee HJ, Hong MK, Ham SD, Cho SH, Moon SH (2009) Fouling of an anion exchange membrane in the electrodialysis desalination process in the presence of organic. *Desalination* 238:60–69. <https://doi.org/10.1016/j.desal.2008.01.036>
25. Yang Z, Guo R, Malpass-Evans R, Carta M, McKeown NB, Guiver MD, Wu L, Xu T (2016) Highly conductive anion-exchange membranes from microporous Tröger's base polymers. *Angew Chem Int Ed* 128:11671–11674. <https://doi.org/10.1002/ange.201605916>
26. Hong JG, Zhanf B, Glabman S, Uzal N, Dou X, Zhang H, Wei X, Chen Y (2015) Potential ion exchange membranes and system performance in reverse electrodialysis for power generation: a review. *J Membr Sci* 486:71–88. <https://doi.org/10.1016/j.memsci.2015.02.039>
27. Geis GM, Hickner MA, Logan BE (2013) Ionic resistance and permselectivity tradeoffs in anion exchange membranes. *ACS Appl Mater Interfaces* 5:10294–10301. <https://doi.org/10.1021/am403207w>
28. Cui Y, Chen X, Wang Y, Peong J, Zhao L, Du J, Zhai M (2019) Amphoteric ion exchange membranes prepared by preirradiation-induced emulsion graft copolymerization for vanadium redox flow battery. *Polymers* 11:1482. <https://doi.org/10.3390/polym11091482>
29. P.E. Dlugolecki, (2009) Mass transport in reverse electrodialysis for sustainable energy generation. University of Twente. 978-90-365-2928-0. <https://doi.org/10.3990/1.9789036529280>
30. Choi I, Han JY, Yoo SJ, Henkensmeier D, Kim JY, Lee SY, Han J, Nam SW, Kim JJ, Jang JH (2016) Experimental investigation of operating parameters in power generation by lab-scale reverse electro-dialysis (RED). *Bull Korean Chem Soc* 37:1010–1019. <https://doi.org/10.1002/bkcs.10810>
31. Jeong J, Song H, Choi I (2021) Electrochemical analysis on how structural and compositional modification of electrode affects power generation in reverse electrodialysis. *Korean J Chem Eng* 38:170–178. <https://doi.org/10.1007/s11814-020-0690-3>
32. Zhao Z, Shi S, Cao H, Li Y, Bruggen BV (2019) Comparative studies on fouling of homogeneous anion exchange membranes by different structured organics in electrodialysis. *J Environ Sci* 77:218–228. <https://doi.org/10.1016/j.jes.2018.07.018>
33. H.J. Lee, S.H. Moon, (2000) A study on characterization of anion exchange membranes in electrodialysis of silica-containing solution. The Membrane Soc. of Korea (Fall Meeting) 79–82.
34. Strathmann H, Grabowski A, Eigenberger G (2013) Ion-exchange membranes in the chemical process industry. *Ind Eng Chem Res* 52:10364–10379. <https://doi.org/10.1021/ie4002102>
35. Guler E, Zhang Y, Saakes M, Nijmeijer K (2012) Tailor-made anion-exchange membranes for salinity gradient power generation using reverse electrodialysis. *ChemSusChem* 5:2262–2270. <https://doi.org/10.1002/cssc.201200298>
36. Kumar M, Singh S, Shahi VK (2010) Cross-Linked Poly(vinyl alcohol)–Poly(acrylonitrile-co-2-dimethylamino ethylmethacrylate) based anion-exchange membranes in aqueous media. *J Phys Chem B* 114:198–206. <https://doi.org/10.1021/jp9082079>
37. Park JS, Choi JH, Woo JJ, Moon S (2006) An electrical impedance spectroscopic (EIS) study on transport characteristics of ion-exchange membrane systems. *J Colloid Interface Sci* 300:655–662. <https://doi.org/10.1016/j.jcis.2006.04.040>
38. Fontannaova E, Zhang W, Nicotera I, Simari C, Baak W, Profio GD, Curcio E, Drioli E (2014) Probing membrane and interface properties in concentrated electrolyte solutions. *J Membr Sci* 459:177–189. <https://doi.org/10.1016/j.memsci.2014.01.057>
39. Shi X, Field R, Hankins N (2012) Review of fouling by mixed feeds in membrane filtration applied to water purification. *Desalination Water Treat* 35:68–81. <https://doi.org/10.5004/dwt.2011.3131>
40. Wang W, Fu R, Liu Z, Wang H (2017) Low-resistance anti-fouling ion exchange membranes fouled by organic foulants in electrodialysis. *Desalination* 417:1–8. <https://doi.org/10.1016/j.desal.2017.05.013>
41. Zhang L, Jia H, Wang J, Wen H, Li J (2020) Characterization of fouling and concentration polarization in ion exchange membrane by *in-situ* electrochemical impedance spectroscopy. *J Membr Sci* 594:117443. <https://doi.org/10.1016/j.memsci.2019.117443>
42. Yu CH, Fang LC, Lateef SK, Wu CH, Lin CF (2010) Enzymatic treatment for controlling irreversible membrane fouling in cross-flow humic acid-fed ultrafiltration. *J Hazard Mater* 177:1153–1158. <https://doi.org/10.1016/j.jhazmat.2010.01.022>
43. Katsoufidou K, Yiantsios SG, Karabelas AJ (2008) An experimental study of UF membrane fouling by humic acid and sodium alginate solutions: the effect of backwashing on flux recovery. *Desalination* 220:214–227. <https://doi.org/10.1016/j.desal.2007.02.038>
44. Jermann D, Pronk W, Meylan S, Boller M (2007) Interplay of different NOM fouling mechanisms during ultrafiltration for drinking water production. *Water Res* 41:1713–1722. <https://doi.org/10.1016/j.watres.2006.12.030>

Publisher's Note Springer Nature remains neutral with regard to jurisdictional claims in published maps and institutional affiliations.

Springer Nature or its licensor (e.g. a society or other partner) holds exclusive rights to this article under a publishing agreement with the author(s) or other rightsholder(s); author self-archiving of the accepted manuscript version of this article is solely governed by the terms of such publishing agreement and applicable law.

Authors and Affiliations

Heajung Song¹ · Insoo Choi^{1,2} 

¹ Department of Energy and Chemical Engineering,
Kangwon National University, 346 Jungang-ro, Samcheok,
Gangwon-do 25913, Republic of Korea

² Division of Energy Engineering, Kangwon National
University, 346 Jungang-ro, Samcheok, Gangwon-do 25913,
Republic of Korea